Turk J Phys
29 (2005) , 307 – 318.

A Theoretical Study on Silicon and III-V Compound Nanotubes

Engin DURGUN, Salim ÇIRACI
Department of Physics, Bilkent University, Bilkent
Ankara 06800, TURKEY

Received 10.10.2005

Abstract

In this paper we present a theoretical study on single-wall silicon and III-V compound nanotubes. First principles plane wave calculations within density functional theory are used to predict energetics and electronic structures of armchair and zigzag nanotubes. The stability of tubular structures is further investigated at finite temperature by *ab initio* molecular dynamics calculations. Our results indicate that (n,0) zigzag and (n,n) armchair single-wall Si nanotubes are stable for $n \geq 6$. Mechanically, the Si nanotubes are radially soft, however they are strong against axial deformations. Electronic analysis showed that zigzag nanotubes are metallic for $n \leq 11$, but they show semiconducting behavior for larger radii. On the other hand, all armchair nanotubes are metallic. (8,0) single wall nanotube has been chosen as prototypes for AlP, GaN, and GaAs compounds and we found that they are semiconducting and stable at room temperature.

Key Words: silicon, nanotube, first principles calculations

1. Introduction

Carbon nanotubes [1] are unique one dimensional nanostructures since they posses exceptional physical properties [2, 3, 4]. They can be functionalized by adsorption of adatoms and molecules. They are considered as base materials for the fabrication of molecular switches, superstrong fibers, high-conducting nanowires, and nanomagnets [5].

As far as the electronic applications are concerned, silicon possesses some properties superior to carbon; it has excellent mechanical properties, high affinity and stability to acid. Moreover, a well-advanced and feasible device technology has been developed for decades for materials based on bulk Si. While the use of carbon based structures such as single-wall carbon nanotubes (SWCNT) requires a completely new paradigms in the development of nanodevices, Si still continues to attract interest for technological applications in nanotechnology. Therefore, Si based nanowires and nanotubes have been subject of experimental and theoretical analysis.

Even if a single-wall Si nanotube (SWSiNT) has never been observed, theoretical predictions have been performed for various kinds of Si tubes. Fagan *et al.* [6, 7] have investigated the structural and electronic properties of chiral SWSiNTs based on Density Functional Theory (DFT) and found that their electronic properties depend on their chirality. Barnard *et al.* [8] have examined the dependence of heat of formation and binding energy of SWSiNTs on their radius and chirality. The stability of (10,0) SWSiNT has been examined by using empirical Monte-Carlo molecular dynamics method and found that it is stable at finite temperature [7]. Ponomarenko *et al.* [9] studied the energetics and relative stability of infinite and finite, clean and hydrogenated open-ended Si nanotubes by using the extended Brenner potential. The existence of H-doped stable tube-shaped finite SiNTs have been predicted [10] and their electronic structures have been

compared with carbon nanotubes [11]. Seifert *et al.* [12] have argued that structures of silicate and SiH nanotubes are more stable than bare Si nanotubes. They studied their mechanical and electronic properties using DFT tight-binding (TB) method and concluded that all these structures are semiconducting. Recently, the successful synthesis of multiwalled Si nanotubes by the use of the method of vapor deposition within nanochannels of Al_2O_3 has been reported by D.Niu *et. al.* [13]. Now, SWSiNTs are no longer hypothetical structures and it is not unrealistic to expect their fabrication with controllable size and diameter.

Similarly, achievement of synthesis of nanotubes such as BN [14] and GaN [15, 16] has increased the interest in the theoretical analysis of compound nanotubes [17, 18]. In addition, the synthesis of Mo and W chalcogenid nanotubes [19, 20, 21], and also NiCl tubular and cage structures have been realized [22]. In order to guide further experimental research aiming at the synthesis of various tubular structures of group IV elements and III-V compounds more theoretical studies concerning their energetics, and stability under radial deformation and at high-temperature are necessary.

In this paper we present a theoretical analysis of Si-nanotubes and III-V compound nanotubes based on state-of-the-art first-principles calculations. Our work is concentrated mainly on the tube structures which can be viewed as the rolling of graphenelike honeycomb planes of Si or III-V elements on a cylinder of radius R. Starting from the precursor graphenelike honeycomb structures we investigated their stability, energetics, and electronic properties of these nanotubes. Since O, O_2, Si, Au and H are critical elements for various processes on Si, we also examined the adsorption of these atoms on SWSiNT. The (8,0) zigzag tubes of AlP, GaN, and GaAs are stable and semiconducting. The results obtained from the present study have been compared systematically with those of SWCNT. The stable tube structures predicted in this study are hoped to motivate experimental research aiming at the synthesis of various tubular structures of group-IV elements and III-V and II-VI compounds.

2. Method

We have performed first-principles plane wave calculations [23, 24] within DFT [25] using ultra-soft pseudopotentials [24, 26]. The exchange correlation potential has been approximated by generalized gradient approximation (GGA) [27]. All structures have been treated by supercell geometry using the periodic boundary conditions. To prevent interactions between adjacent structures a large spacing ($\sim 10\mathring{A}$) has been taken. Convergence with respect to the number of plane waves used in expanding Bloch functions and **k**-points in sampling the Brillouin zone are tested for the parent bulk crystals as well as tubular structures. In the self-consistent potential and total energy calculations the Brillouin zone of nanotubes has been sampled by (1x1x19) mesh points in **k**-space within Monkhorst-Pack scheme [28]. Calculations of graphene and graphite structures have been carried out using (19x19x1) and (8x8x6) **k**-point samplings, respectively. A plane-wave basis set with kinetic energy cutoff $200eV \leq \hbar^2|\mathbf{k}+\mathbf{G}|^2/2m \leq 330eV$ has been used. All atomic positions and lattice parameters are optimized by using the conjugate gradient method where total energy and atomic forces are minimized. The convergence for energy is chosen as 10^{-5} eV between two ionic steps, and the maximum force allowed on each atom is 0.05 eV/$\mathring{A}$.

The stability of the structures we studied is the most crucial aspect of our work, since it provides valuable information for the synthesis of these materials in the future. In this respect an extensive analysis of stability has been carried out for various nanotubes. First, we applied a radial deformation to certain nanotubes and optimized their structures to see whether they relax to their original, undeformed circular forms under zero external force. Furthermore, we have performed, finite temperature *ab initio* molecular dynamics calculations up to 1000 K using the Nosé thermostat [29] for 250 time steps (0.5 ps) to check whether the optimized structure will be affected from random thermal motion of atoms or whether they maintain their tubular form at high temperatures. We believe that if there were any kind of structural instability it would be initiated and also enhanced within these time steps at high temperatures.

3. Honeycomb structure of silicon and III-V compounds

One of the main difficulties for synthesizing Si nanotubes seems to be the absence of 2D silicon layer similar to the graphene structure of carbon. This is traced to the fact that in contrast to carbon, sp^3-

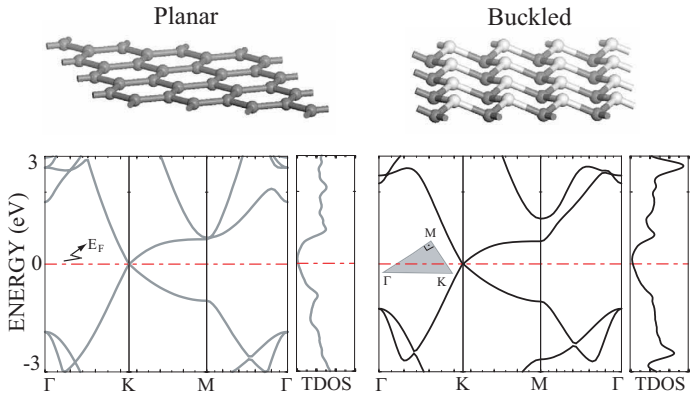

Figure 1. Band structure and total density of states (TDOS) analysis for planar and buckled honeycomb structure (HC) of Si. Light-lines correspond to planar (having P6/MMM symmetry) and dark-lines correspond to buckled structure (having P-3M1 symmetry). The zero of energy is set to the Fermi level E_F. The inset shows the 1/12 of hexagonal Brillouin zone.

hybridization in Si is more stable than sp^2-hybridization [30]. In view of this situation, we examined whether the graphenelike 2D sheet of silicon can be stable. Two dimensional hexagonal lattice forming a honeycomb structure in the xy-plane has been periodically repeated along the z-axis with 10 $\AA$ spacing to minimize interlayer interactions. In order to reduce the effects of the constraints to be imposed by using the primitive unit cell we performed structure optimizations on the (2x2) cell in the xy-plane. Our calculations revealed that the planar structure (where all atoms lie in the same plane) is metastable, but it is buckled by a 0.45 $\AA$ relative vertical displacement of alternate atoms on the hexagons. The gain of energy upon buckling is 30 meV/atom. The binding energy is calculated to be 4.9 eV/atom which is 0.6 eV lower than the Si diamond structure and the average distance between nearest Si atoms is 2.2$\AA$. In the rest of the paper, this graphenelike structure will be specified as the buckled honeycomb structure. As shown in Figure 1, the detailed band structure and total density of states (TDOS) analysis indicate that both buckled and planar systems have large band gaps along ΓK and MK directions, but conduction and valence bands cross the Fermi level at the **k**-point of the Brillouin zone. The electronic structure of the system does not change significantly as a result of buckling, except some of the bands split due to the lowering of the rotation symmetry. Using a similar method but different pseudopotentials and an exchange correlation potential, Takeda and Shiraishi [31] have examined planar and buckled honeycomb structures of Si. Our results, obtained in a four times larger cell, hence allowing more variational freedom are in overall agreement with the results in Ref. [31]. Moreover, we performed an *ab initio* molecular dynamics calculations on 2x2 supercell providing further evidence that the buckled honeycomb structure is stable at 500K for 250 time steps.

Next we address whether a graphite like structure of Si (or graphitic Si) can form. Our study distinguished chemisorption and physisorption states in the interlayer interaction, in contrast to only the physisorption state in graphite [32]. The chemisorption state corresponding to a smaller lattice parameter $c = 6\AA$ is energetically more favorable, namely the binding is 5.1 eV which is 0.4 eV smaller than that of the bulk Si. We note, however, that the lattice parameters and the binding energies depend on the approximation of exchange-correlation potential [33, 34].

Similar to Si, the honeycomb structures of AlP, GaAs and GaN are found to be stable also, but less energetic relative to the bulk crystal by 0.8, 1.1 and 0.6 eV per basis, respectively. However, the buckling is not favored in order to hinder the formation of a dipole layer.

4. Single wall silicon nanotubes

4.1. Energetics and Stability

Having discussed the stability of a buckled Si honeycomb structure (Si-HC), now we present our systematic analysis of $(n,0)$ zigzag and (n,n) armchair SWSiNTs for different n values; namely $n = 3-14$ for zigzag and $n = 3, 6, 9$ for armchair structures. The (3,0) zigzag SWSiNT has clustered upon structure relaxation, indicating that it is not stable even at T=0 K. While the structure optimization has resulted in regular (4,0) and (5,0) tubular structures, the *ab initio* MD calculations showed that these nanotubes eventually transform into clusters at higher temperatures as shown in Figure 2. Significant distortions can be easily noticed in (6,0) and also (7,0) SWSiNTs, but tubular character and hexagonal structures on the surface have remained. The (6,0) zigzag tube, which has a radius of $R = 3.8\mathring{A}$ as well as those with larger radii remain stable at temperatures up to 800 K. Barnard and Russo [8] also reported the instability of (3,0) SWSiNT in their first-principles study, but they considered (4,0) and (5,0) SWSiNTs as stable structures depending on their geometry optimization performed at T=0 K. Present results set a limit for fabricating small radius SWSiNTs. The first and second nearest neighbor interactions between Si atoms become relevant for the stability of small radius nanotubes and causes clusterings, if $R < 3.8\mathring{A}$. Similar behavior is also obtained for (n,n) armchair SWSiNTs. For example (3,3) SWSiNT is clustered at 800 K in spite of the fact that geometry optimization yields tubular structure at T=0 K. On the other hand, the (6,6) tube with a relatively larger radius remained stable at 800 K after 250 time steps. In contrast to (n,n) SWSiNTs, which are found unstable for $n < 6$, the (3,3) SWCNT is known to be stable and experimentally fabricated [35, 36]. The difference in the chemical behavior of C and Si can be traced to the difference in their π-bonding capabilities. Si tends to utilize all of its three valence p-orbitals, resulting in sp^3-hybridization. In contrast, the relatively large promotion energy from C-*2s* to C-*2p* orbitals explains how carbon will activate one valence p-orbital at a time leading, in turn, to sp, sp^2, sp^3-hybridizations in 1D, 2D and 3D structures. This is the explanation why tubular structures of C are more stable than those of Si [11]. Moreover, since the interatomic distance increases significantly in going from C to Si, the $\pi - \pi$ overlap decreases accordingly, resulting in much weaker π-bonding for Si tubes in comparison with that for carbon tubes.

After the discussion of stability, we next analyze the energetics, namely the behavior of binding energy (E_b) as a function of the radius (or n) of the tube. E_b per atom is calculated using the expression,

$$E_b = \{E_T[SWSiNT] - N(E_T[Si])\}/N \tag{1}$$

in terms of the total energy of the optimized SWSiNT having N Si atoms per unit cell, $E_T[SWSiNT]$, and the total energy of N, free Si atom $E_T[Si]$. It is found that $E_b \sim 4.9$ eV and slightly increases as the radius R (or n) increases for both zigzag and armchair SWSiNTs as displayed in Figure 3. The energy increase with n is small. According to our results E_b's of (n,n) armchair SWSiNTs are ~ 0.05 eV larger than those of $(n,0)$ zigzag ones because of their relatively larger radius at a given n. Corresponding E_b for SWCNTs is calculated to be 9.1 eV [37] theoretically.

Finally, the strain energy per atom is calculated relative to the energy of the honeycomb structure,

$$E_S = E_b[SWSiNT] - (E_b[Si - HC]) \tag{2}$$

by subtracting the binding energy (per atom) of optimized honeycomb structure, $E_b[Si - HC]$ from the binding energy of SWSiNT. A slight increase in strain energy is observed as the radius R or n decreases. This is an expected result, since the structure becomes more graphenelike with the increasing radius. Calculated strain energies given by the inset in Figure 3 are also in agreement with the results obtained by Fagan *et al.* [7] and Barnard and Russo [8]. Calculated value of the strain energy of a zigzag SWSiNT is smaller than the strain energy of a zigzag SWCNT having comparable radius [38]. In the classical theory of elasticity the strain (or curvature) energy of a tubular structure is given by the expression $E_S = \alpha/R^2$, where α is a function of Young's modulus and thickness of the tube's wall [5, 39]. The result of the present calculations in Figure 3 gives a fair fit to the expression, α/R^2 with $\alpha \sim 2.07 eV/\mathring{A}^2$.

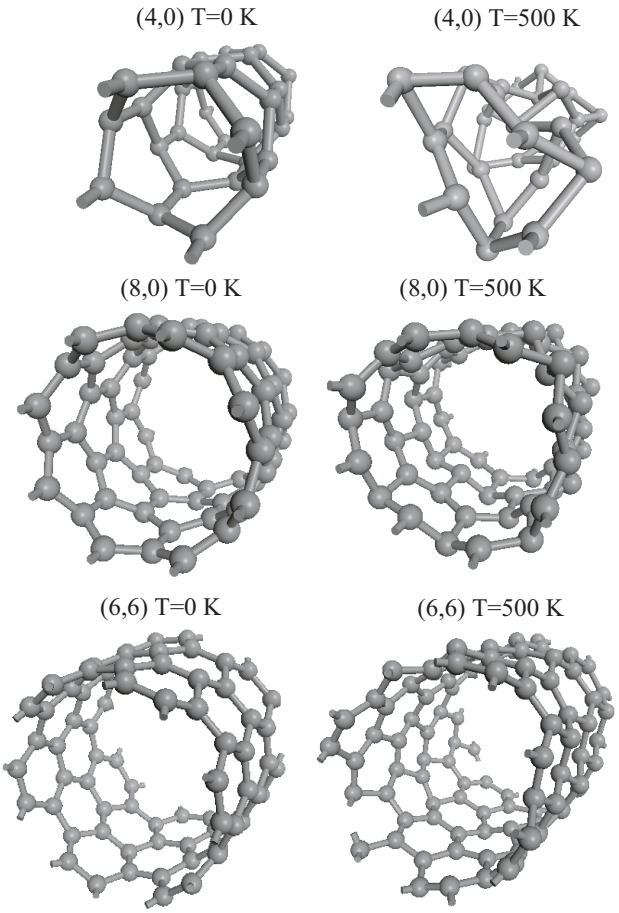

Figure 2. Structures of (4,0), (8,0) and (6,6) SWSiNTs at T=0 and T=500K after 250 time steps. A tubular structure has remained in (6,6) and (8,0) SWSiNT, but the (4,0) structure has clustered.

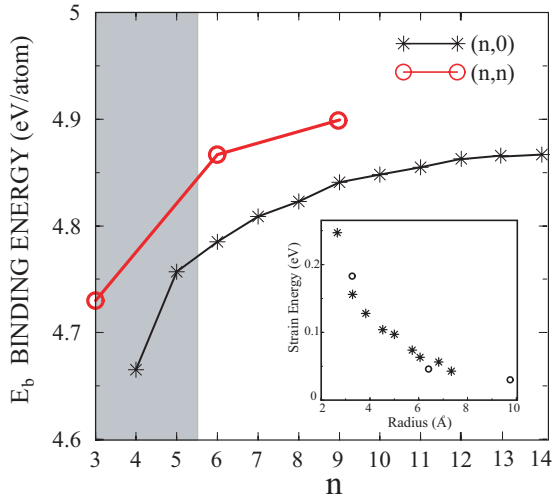

Figure 3. The calculated binding energy per atom for $(n, 0)$ zigzag and (n, n) armchair SWSiNTs. The dark region indicates that tubular structures are unstable at finite temperature. The calculated strain energies E_S per atom for $(n, 0)$ and (n, n) SWSiNTs are shown in the inset.

4.2. Mechanical Properties

Radial flexibility is a criterion for the stability of tubular structure. SWCNTs are known to be flexible for the deformations in radial directions [40, 41]: they can sustain severe radial deformation transforming the circular cross section into an elliptical one with minor (b) and major (a) axes. The radial deformation on a bare tube of radius R is specified in terms of the strain associated with the pressing of the tube along the minor axis, $\epsilon_{yy} = (b - R)/R$ and the strain associated with the expansion of the tube along the perpendicular major axis $\epsilon_{xx} = (a - R)/R$. Theoretical and experimental research has shown that radially deformed tubes relax reversibly to the original circular cross section whenever the external radial force is lifted [42]. Moreover, radial deformation can modify the electronic structure reversibly, which leads to a tunable band gap engineering [42, 43]. For example, a semiconducting (n,0) can be metallic under radial deformation. Our results indicate that SWSiNTs display a behavior different than that of SWCNTs. We performed a systematic analysis of radial strain for (8,0) zigzag and (6,6) armchair SWSiNTs. First, these tubes have been deformed by applying ϵ_{yy}=-0.1,-0.2, and -0.3. Then the stress (or constraint) imposing these radial strains has been lifted and the structure has been optimized. Contrary to the situation in carbon nanotubes, up to the applied strain $\epsilon_{yy} \leq$-0.2 the SWSiNTs have remained in the deformed state. For example, (8,0) tubes with an initial radial strain of ϵ_{yy}=-0.1 and -0.2 are relaxed to a plastic deformation corresponding to ϵ_{yy}=-0.09 and ϵ_{yy}=-0.14, respectively. Similar results have been obtained for (6,6) armchair SWSiNT with initial radial strain of ϵ_{yy}=-0.1 and -0.2. In contrast, the tubes, which initially strained by ϵ_{yy}=-0.25 and -0.3 have relaxed to a state with negligible residual strain. The total energy of the undeformed SWSiNT E_T^o have been found to be lower (more energetic) than the total energy $E_T^r(\epsilon_{yy})$ of tubes which were relaxed upon radial deformation $-0.3 \leq \epsilon_{yy} \leq 0$. However, the energy difference $\Delta E = E_T^r(\epsilon_{yy}) - E_T^o > 0$ is very small. The weakness of π-bonds of Si as compared to carbon nanotubes is possibly a reason why the restoring forces are not strong enough to derive the deformed state to relax back to the original undeformed state. Once the applied radial deformation gets significant ($|\epsilon_{yy}| > 0.2$) the restoring forces become strong enough to derive the relaxation towards circular cross section. On the other hand, after a severe radial strain that causes a significant coupling between opposite internal surfaces the deformed state may be more energetic (*i.e* $E_T^r(\epsilon_{yy}) < E_T^o$ or it may relax to different structures such as clusters. This situation constitutes an important difference between Si and C single-wall nanotubes.

The axial strength of SWSiNT, or the elastic stiffness along tube axis is defined as the second derivative of the strain energy per atom with respect to the axial strain ϵ_{zz}, namely $\kappa = d^2E_T/d\epsilon_{zz}^2$. The elastic stiffness of the (8,0) SWSiNT along its axis is calculated to be 23 eV. This value is significant, but smaller than that of SWCNT which is calculated to be 52-60 eV [44].

4.3. Electronic Structure

A systematic analysis of the electronic structure indicates that metallic zigzag SWSiNTs $6 \leq n \leq 11$ have three bands crossing the Fermi level, but a band gap between the valence and conduction bands opens when $n \geq 12$. A similar effect has been obtained for zigzag SWCNTs when $n \geq 7$ [5, 38]. This metal-semiconductor transition was attributed to the energy shift of the singlet π^*-band which is normally empty, but becomes filled due to increased $\sigma^* - \pi^*$ hybridization at a small radius [38, 45]. In the present case it appears that $\sigma^* - \pi^*$ hybridization becomes significant at a relatively larger radius. The conductance of all these infinite, perfect tubes ($6 \leq n \leq 11$) is predicted to be equal to $3G_o$ ($G_o = 2e^2/\hbar$). Similar metallic behavior is also obtained for armchair types namely for (6,6) and (9,9) SWSiNTs. The conductance of ideal infinite (n, n) tubes is $2G_o$, but not $3G_o$ as in metallic $(n, 0)$ zigzag tubes. Figure 4 presents the systematic analysis of $(n, 0)$ tubes for $7 \leq n \leq 14$ and clearly shows how the singlet π^*-band gradually raises as R increases.

Based on LDA calculations Fagan *et al.* [6, 7] also found (6,6) and (6,0) SWSiNT's metallic, but they predicted (10,0) and (12,0) zigzag nanotubes are semiconductor with a small band gap of 0.1 eV. The disagreement between the present one and those of Fagan *et al.* [6, 7] may be due to the differences in pseudopotentials and in the approximation of exchange correlation potential. Electronic structure analysis performed for the tubes under strain both radially and axially showed that the metallic character is not altered but the position of the Fermi level is slightly changed due to deformation. The modification of the electronic structure with chirality may offer the possibility of fabrication of nanodevices using SWSiNT junctions. On the other hand, SWSiNTs can be used as metallic interconnects, since their conductance is not severely affected by deformation.

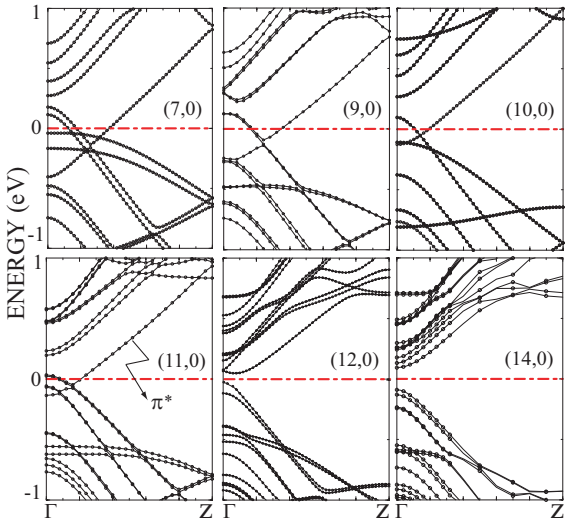

Figure 4. The energy bands calculated for (7,0), (9,0), (10,0), (11,0),(12,0), and (14,0) SWSiNTs using GGA. The lowest conduction band, or singlet π^*-band, is indicated. The zeros of energy are set at the Fermi level.

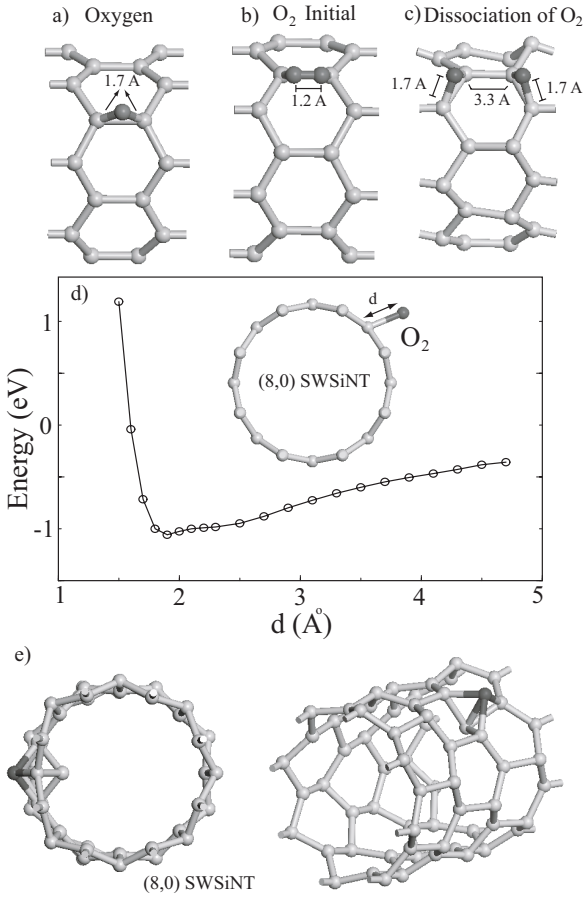

Figure 5. (a) The optimized geometry of an O atom adsorbed over the axial site of (8,0) SWSiNT. (b) Initial adsorption geometry of O_2 over the axial site. (c) Dissociation of O_2 after relaxation and formation of Si-O-Si bridge bands over the adjacent zigzag Si-Si bonds. (d) Variation of interaction energy as a function of the distance d of an O_2 molecule from the parallel axial Si-Si band. (e) Optimized geometry of a single Si atom adsorbed on the top site (indicated by a dark ball).

4.4. Interaction of SWSiNT with Atoms and Molecules

The interaction of Si nanotubes with an oxygen atom and an oxygen molecule is extremely important for technological applications. The adsorption of an oxygen atom is studied by placing it initially above a Si-Si bond parallel to the axis of a (8,0) SWSiNTs. The optimized structure shown in Figure 5(a). has a very strong chemical bonding between O and SWSiNT with E_b=8.1 eV and the nearest Si-O distance 1.7 $\mathring{A}$. The resulting geometry showed that SWSiNT is slightly distorted upon O adsorption.

The interaction between O_2 and SWSiNT has been revealed by calculating the binding energy as a function of the separation d from the axial Si-Si bond of the tube as shown in Figure 5(b). The O_2 molecule is kept unrelaxed and taken parallel to the Si-Si bond. The calculated energy versus distance curve $E(d)$ in Figure 5(d) shows that O_2 can be attracted to the tube, but there is no physisorption state as in O_2+SWCNT [46]. The minimum of $E(d)$ occurs at 1.9 $\mathring{A}$. Upon relaxation of the tube and O_2 near this minimum, the molecule has been dissociated to form two Si-O-Si bridge bonds over the zigzag Si-Si bonds, and concomitantly SWSiNT has been distorted locally as illustrated in Figure 5(c). The distances between nearest Si-O and O-O are 1.7 and 3.3 $\mathring{A}$, respectively. We repeated the structure relaxation by initially placing O_2 at a larger distance $d = 2.5\mathring{A}$ from the surface of the tube and we obtained the same dissociated state. Our results indicate that there will be a strong interaction between the Si nanotube and the oxygen molecule in open air applications.

The SWSiNT surface is found to be reactive against Si, H, and Au atoms. The Si atom attached to the top site is bound by $E_b \sim 5$ eV. One Si atom of the tube is plunged inside the tube and a small cluster is formed at the surface [see Figure 5(e)]. The chemisorption energy of H and Au atoms is strong and found to be 4.4 eV and 3.4 eV, respectively.

5. Single wall nanotubes of III-V compounds

Motivated by interesting properties of SW(BN)NT and opto-electronic and field emitting properties of GaN and AlN tubular forms [16, 47] we choose (8,0) AlP, GaAs, and GaN single-wall nanotubes as prototypes to investigate the stability and electronic properties of III-V compound nanotubes. Even if the single-wall nanotubes of these compounds have not been sythesized yet, the predictions of the present work are essential for further efforts to achieve it. The initial bond lengths are chosen as the distance between nearest cation and anion atoms in bulk structure. After relaxation of all atomic positions, as well as lattice constant c, the tubular structures remained stable. The *ab initio* MD calculations also showed that SW(AlP)NT remained stable at room temperature after 250 time steps. E_b is calculated to be 9.6 eV per AlP basis. The radius of the tube is 5.2 $\mathring{A}$. The structure is not a perfect tube but the hexagons on the surface are buckled. The nearest Al-P distance is $2.3\mathring{A}$, and second nearest neighbor distance *i.e*, nearest P-P and Al-Al distances are $3.9\mathring{A}$ and $3.8\mathring{A}$, respectively. The energy band and TDOS analysis in Figure 6 points out that (8,0) SW(AlP)NT is a semiconductor (insulator) with a band gap of 2.0 eV.

Initial tubular structure of (8,0) SW(GaAs)NT is maintained after geometry optimization at T=0 K. Similar to SW(AlP)NT, hexagons are buckled. E_b is calculated to be 7.7 eV per GaAs and the radius is 4.8 $\mathring{A}$. The nearest Ga-As distance is $2.4\mathring{A}$, and nearest Ga-Ga and As-As distances are $3.9\mathring{A}$ and $4.1\mathring{A}$, respectively. The (8,0) SW(GaAs)NT is also a semiconductor (insulator) with a band gap of 0.9 eV.

We place a special emphasis on GaN nanotubes,[16, 48] which are successfully synthesized by an epitaxial casting method where ZnO nanowires are initially used as templates. GaN nanotubes produced this way have a diameter of 300 $\mathring{A}$ and a minimum wall thickness of 50 $\mathring{A}$. They are semiconducting and hence they would be a possible candidate for opto-electronic applications. Whether a single-wall GaN tube of smaller diameter ($2R \sim 10\mathring{A}$) can be stable and can exhibit technologically interesting electronic properties is important to know. We again took (8,0) SW(GaN)NT as a prototype for the sake of consistency. Stable tubular geometry is obtained by both geometry optimization at T=0 K and *ab initio* MD analysis at T=800 K. Upon relaxation atoms on the surface are buckled. E_b is calculated to be 11.5 eV per GaN and the radius is 4.1 $\mathring{A}$. The nearest Ga-N distance is $1.8\mathring{A}$, and the nearest Ga-Ga and N-N distances are $3.1\mathring{A}$ and $3.2\mathring{A}$, respectively. We found that the (8,0) SW(GaN)NT is a semiconductor (insulator) with a band gap of 2.2

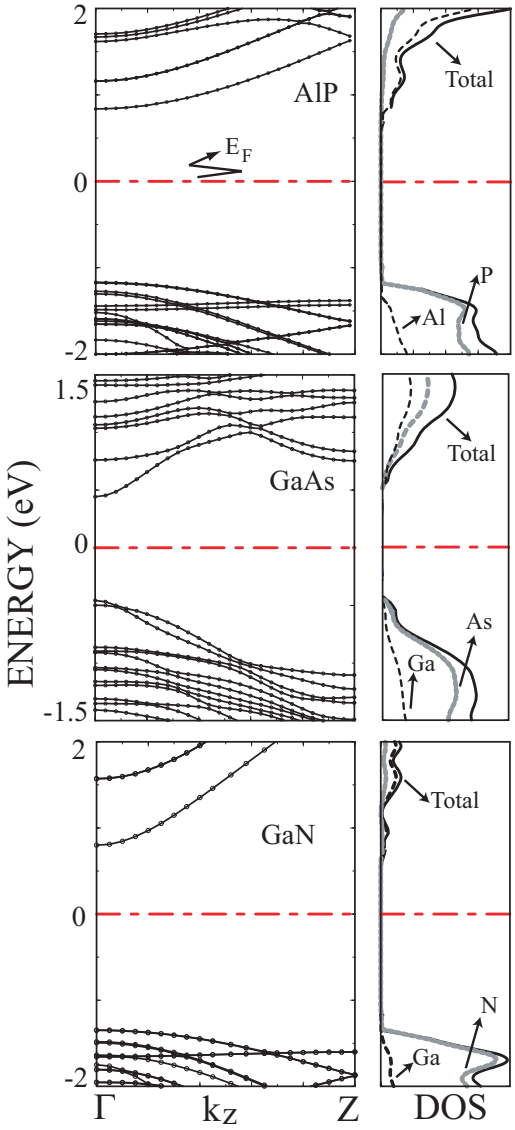

Figure 6. Energy band structures (left panels),total density of states (TDOS) and partial density of states (PDOS) on atoms (right panels) of (8,0) zigzag SW(AlP)NT, SW(GaAs)NT, and SW(GaN)NT. Anion (Al, Ga) and cation (P, As, N) contributions to TDOS are shown by dashed and light-continuous lines. Zero of the energy is set at the Fermi level.

eV. A previous first-principles study performed by Lee et al. [17] by using LDA method predicted the similar band gap for SW(GaN)NT. Here, we examine also whether SW(GaN)NT is radially elastic. To this end we started with the elliptically deformed nanotube under $\epsilon_{yy} = -0.1$, and let it relax in the absence of radial forces. Similar to the Si nanotube, SW(GaN)NT is found to be radially soft.

6. Conclusion

In this paper, we analyzed the stability of Si and III-V compound, single-wall nanotubes, and calculated their optimized atomic structure and energy band structure. Si as well as III-V compounds can form stable a 2D honeycomb structure, which is precursor of nanotubes. The energy necessary to roll these honeycomb structures over a cylinder of radius R to make a perfect nanotube is however small as compared to those in

carbon nanotubes. We found that Si single-wall nanotubes with small radius are unstable and are clustered either at T=0 K or at finite temperatures. For example, while (3,0) is unstable even at T=0 K, (4,0) and (5,0) lose their tubular character and tend to form cluster at T=500 K. Stable $(n, 0)$ zigzag SWSiNTs are metallic for $6 \leq n \leq 11$, but become semiconducting for $n \leq 12$. The metallicity of small radius $(n, 0)$ tubes is a typical curvature effect and results from the dipping of the singlet π^*-band into the valence band at small radius. Stable (n, n) armchair SWSiNTs (n=6,9)are metallic. Our study on radially deformed (8,0) and (6,6) SWSiNTs demonstrated that these nanotubes are radially "soft", and hence are devoid of the strong restoring force that maintains radial elasticity. The radial softness of Si tubes is a behavior which distinguishes them from carbon nanotubes. In contrast to that axial stiffness the Si nanotube has been found to be high. We predicted that oxygen molecule adsorbed on the Si-Si bonds dissociates. A strong interaction between O/O_2 and SWSiNT appears to be serious in future processes involving Si tubes. Adatoms like Si, Au, and H can also form strong chemisorption bonds with the atoms on the surface of SWSiNT. Finally, we found III-V compound (8,0) nanotubes (AlP, GaAs, and GaN) stable at least at room temperature and they are semiconductors with band gaps ranging from 0.9 eV to 2.2 eV. In contrast to small radius metallic Si nanotubes, (8,0) compound nanotubes are semiconductors. The band gap increases with a decreasing row number of elements. Even though not all the structures treated in this study have been realized experimentally, the predictions obtained from the present first-principles calculations are expected to be essential for further research in this field.

Acknowledgements

Part of the computations have been carried out at ULAK-BIM High Performance Computer Center. SC acknowledges partial financial support from Academy of Science of Turkey.

References

[1] S. Iijima, *Nature*, **354**, (1991), 56; S. Iijima , T. Ichihashi and Y. Ando *Nature*, **356**, (1992), 776.

[2] M. S. Dresselhaus, G. Dresselhaus, and P. C. Eklund, *P C Science of Fullerenes and Carbon Nanotubes* (San Diego, CA: Academic), (1996).

[3] R. Saito, G. Dresselhaus, M. S. Dresselhaus, *Physical Properties of Carbon Nanotubes* (London: Imperial College), (1998).

[4] J. W. Mintmire, B. I. Dunlap, and C. T. White, *Phys. Rev. Lett.*, **68**, (1992), 631.

[5] S. Ciraci, T. Yildirim, S. Dag, O. Gülseren, R. T. Senger, *J. Phys.: Condens. Matter*, **16**, (2004), R901.

[6] S. B. Fagan, R.J. Baierle, R. Mota, A. J. R. da Silva and A. Fazzio, *Phys Rev. B*, **61**, (1999), 9994.

[7] S. B. Fagan, R. Mota, R. J. Baierle, G. Paiva, A. J. R da Silva, and A. Fazzio, *J. Mol. Struct. Theochem*, **539**, (2000), 101.

[8] A. S. Barnard and S. P Russo, *J. Phys. Chem. B*, **107**, (2003), 7577.

[9] O. Ponomarenko, M. W. Radny, and P. V. Smith, *Surface Science*, **562**, (2004), 257.

[10] M. Zhang, Y. H. Kan, Q. J. Zang, Z. M. Su, R. S Wang, *Chem. Phys. Lett.*, **379**, (2003), 81.

[11] R. Q. Zhang, S. T Lee, C. K. Law, W. K. Li, and B. K. Teo, *Chem Phys. Lett.*, **364**, (2002), 251.

[12] G. Seifert, Th. Köhler, K. H. Urbassek, E. Hernàndez, and Th. Frauenheim, *Phys Rev. B*, **63**, (2001), 193409.

[13] J. Sha, J. Niu, X. Ma, J. Xu, X. Zhang, Q. Yang and D. Yang, *Adv. Mater*, **14**, (2002), 1219; J. Niu, J. Sha, and D. Yang, *Physica E*, **23**, (2004), 131.

[14] A. Loiseau, F. Willaime, N. Demoncy, G. Hug, and H. Pascard, *Phys. Rev. Lett*, **76**, (1996), 4737.

[15] Z. Liliental-Weber, Y. Chen, S. Ruvimov, and J. Washburn, *Phys. Rev. Lett.*, **79**, (1997), 2835.

[16] J. Goldberger, R. He, Y. Zhang, S. Lee, H. Yan, H. Choi, and P. Yang, *Nature* (London), **422**, (2003), 599.

[17] S. M. Lee, Y. H. Lee, Y. G. Hwang, J. Elsner, D. Porezag, and T. Frauenheim, *Phys. Rev. B*, **60**, (1999), 7788.

[18] M. Cote, M. L. Cohen, and D. J. Chadi, *Phys. Rev. B*, **58**, (1998), R4277.

[19] L. Rapoport, Y. Bilik, Y. Feldman, M. Homyonfer, S.R. Cohen, and R. Tenne, *Nature* (London), **387**, (1997), 791.

[20] Y. Feldman, E. Wasserman, D. J. Srolovitz, and R. Tenne, *Science*, **267**, (1995), 222.

[21] R. Tenne, L. Margulis, M. Genut, and G. Hodes, *Nature* (London) **360**, (1992), 444.

[22] Y. R. Hacohen, E. Grunbaum, R. Tenne, J. Sloand, and J. L. Hutchinson, *Nature* (London), **395**, (1998), 336.

[23] M. C. Payne, M. P. Teter, D. C. Allen, T. A. Arias, and J. D. Joannopoulos, *Rev. Mod. Phys.*, **64**, (1992), 1045.

[24] G. Kresse and J. Hafner, *Phys Rev. B*, **47**, (1993), R558; G. Kresse and J. Furthmuller, *Phys Rev. B*, **54**, (1996), 11169.

[25] W. Kohn and L. J. Sham, *Phys. Rev.*, **140**, (1965), A1133; P. Hohenberg and W. Kohn, *Phys. Rev. B*, **76**, (1964), 6062.

[26] D. Vanderbilt, *Phys. Rev. B*, **41**, (1990), R7892.

[27] J. P. Perdew, J. A. Chevary, S. H. Vosko, K. A. Jackson, M. R. Pederson, D. J. Singh, and C. Fiolhais, *Phys. Rev. B*, **46**, (1992), 6671.

[28] H. J. Monkhorst and J. D. Pack, *Phys. Rev. B*, **13**, (1976), 5188.

[29] S. Nosé, *Mol. Physics*, **52**, (1984), 255.

[30] U. Röthlisberger, W. Andreoni, and M. Parrinello, *Phys. Rev. Lett.*, **72**, (1994), 665.

[31] K. Takeda and K. Shiraishi, *Phys. Rev B*, **50**, (1994), 14916.

[32] Y. C. Wang, K. Scheerschmidt and U. Gosele, *Phys. Rev. B,* **61**, 12864 (2000).

[33] J. C. Charlier, X. Gronze, and J. P. Michenoud, *Europhys. Lett.*, **28**, (1994), 4040.

[34] W. Kohn, Y. Meir, and D. E. Makarov, *Phys. Rev. Lett.*, **80**, (1998), 4153.

[35] Z. K. Tang et al., *Science*, **292**, (2001), 2462.

[36] N. Wang, Z. K. Tang, G. D. Li, and J. S. Chen, *Nature*, **408**, (2000), 50.

[37] E. Durgun, S. Dag, V. K. Bagci, O. Gülseren, T. Yildirim, S. Ciraci, *Phys. Rev. B*, **67**, (2003), R201401; E. Durgun, S. Dag, S. Ciraci, O. Gülseren, *J. Phys. Chem. B*, **108**, (2004), 575.

[38] O. Gülseren, T. Yildirim, and S. Ciraci, *Phys. Rev. B*, **65**, 153405 (2002).

[39] D. H. Robertson, D. W. Brenner, and J. W. Mintmire, *Phys. Rev. B*, **45**, (1992), R12592 ; G. G. Tibbets, *J. Cryst. Growth*, **66**, (1984), 632; K. N. Kudin, G. E. Seuseria, and B. I. Yakobson, *Phys. Rev. B*, **64**, (2001), 235406.

[40] T. W. Tombler, C. W. Zhou, L. Alexseyev, J. Kong, H. J. Dai, L. Lei, C. S. Jayanthi, M. J. Tang, and S. Y. Wu, *Nature*, **405**, (2000), 769.

[41] P. Zhang, P. E. Lammert, and V. H. Crespi, *Phys. Rev. Lett.*, **81**, (1998), 5346.

[42] O. Gülseren, T. Yildirim, S. Ciraci, and C. Kilic, *Phys. Rev. B*, **65**, (2002), 155410.

[43] C. Kilic, S. Ciraci, O. Gülseren and T. Yildirim, *Phys. Rev. B*, **62**, (2000), R16345.

[44] D. Sanchez-Portal, E. Artacho, J. M. Soler, A. Rubio, and P. Ordejon, *Phys. Rev. B*, **59**, (1999), 12678.

[45] X. Blase, L. X. Benedict, E. L. Shirley, and S. G. Louie, *Phys. Rev. Lett.*, **72**, (1994), 1878.

[46] S. Dag, O. Gülseren, T. Yildirim, and S. Ciraci, *Phys. Rev B.*, **67**, (2003), 165424.

[47] V. N. Tondare, C. Balasubramanian, S. Shende, D. S. Joag, V. P. Godbale, and S. V. Bhoraskar, *Appl. Phys. Lett.*, **80**, (2002), 4813.

[48] M. W. Lee, H. C. Hsueh, H.-M. Lin, and C.-C. Chen, *Phys. Rev. B*, **67**, (2003), 161309(R).